Philip, Anish; Dong, Yujiao; Vapaavuori, Jaana; Karppinen, Maarit

Block Copolymer Approach toward Selective Atomic-Layer Deposition of ZnO Films

Published in:
Advanced Engineering Materials

DOI:
10.1002/adem.202300937

Published: 01/02/2024

Document Version
Publisher's PDF, also known as Version of record

Please cite the original version:
Philip, A., Dong, Y., Vapaavuori, J., & Karppinen, M. (2024). Block Copolymer Approach toward Selective Atomic-Layer Deposition of ZnO Films. *Advanced Engineering Materials*, *26*(4), Article 2300937. https://doi.org/10.1002/adem.202300937

ADVANCED ENGINEERING MATERIALS
www.aem-journal.com

Block Copolymer Approach toward Selective Atomic-Layer Deposition of ZnO Films

Anish Philip, Yujiao Dong, Jaana Vapaavuori, and Maarit Karppinen**

High-quality thin films of ZnO fabricated with atomic-layer precision are attracting increasing interest in various applications beyond the conventional semiconductor industry. This has posed new demands for these thin films regarding, for example, the substrate compatibility and substrate-selective deposition. Herein, the impact of different underlining polymer substrates on the film growth characteristics of ZnO coatings fabricated with the atomic-layer deposition (ALD) technique is investigated. The resultant thin films are systematically characterized for the growth rate, crystallinity, surface morphology, hydrophilicity, and electrical conductivity. Most excitingly, based on the understanding gained for the ZnO film growth on the different homopolymer surfaces, nanoscale-patterned block copolymer (BCP) films via spin coating are designed and fabricated to demonstrate block-selective ALD of ZnO on these BCP surfaces. It will be shown that the polyethylene oxide parts of the BCP act as a significantly more passive surface for the ZnO growth than the polystyrene. Altogether, this concept couples two highly controllable methods—atomic-level precision of ALD and nanoscale precision of BCP substrates—into a simple and scalable way of producing diverse nanomaterial patterns.

1. Introduction

Block copolymers (BCPs) have attracted significant interest in research during recent years due to their highly tunable self-assembly schemes based on intermolecular interactions.[1] Most excitingly, the possibility to synergistically tailor the individual polymer components of BCPs allows the creation of unique surface chemistries and structures for, e.g., next-generation energy storage/conversion devices.[2–6] Moreover, polymers are naturally lightweight materials with a high degree of mechanical flexibility and optical transparency, and hence essential ingredients for the increasingly important future application field of flexible (opto)electronics. Indeed, polymer-based substrates and templates would have many apparent advantages over the more conventional alternatives such as thin metal and plastic foils.[7]

Currently, the n-type II–VI semiconductor ZnO is strongly emerging as a viable material candidate for various micro-, opto-, and piezoelectronic devices, as well as advanced gas sensor and spintronics applications owing to its wide bandgap, visible-light transparency, and stability.[8–13] The visible-light transparency of ZnO is particularly beneficial considering its potential application as a transparent electrode in solar cell applications.[14] Besides its attractive set of physical properties, ZnO is a raw-material-wise and biocompatible material.[8,10,13,15] For the frontier applications of ZnO, high-quality thin films are needed.

Atomic-layer deposition (ALD) has been the fastest growing thin-film technology in conventional microelectronics already for decades,[16–18] and it has also numerous advantages relevant to the growth of high-quality inorganic coatings on polymer substrates for the next-generation flexible applications.[19,20] It has also been used in the context of BCPs.[21–24] The unique way of separating the different precursor gas doses in ALD by sequential precursor pulsing and inert gas purging enables the growth of homogeneous pinhole-free thin films with atomic-layer accuracy even on large-area surfaces.[17,19] Moreover, owing to the high reactivity of ALD precursors, these films can be deposited under relatively mild conditions, even at room temperature,[25–27] which makes the technique compatible with sensitive substrates such as polymers[28–32] for various applications including gas barrier layers for food or medicine package[33–36] and in flexible electronics. It should be also emphasized that ZnO is one of the prototype ALD materials for which the deposition process/parameters from diethyl zinc (DEZ) and water precursors are well established for conventional substrate materials (silicon, glass).[8,13] Moreover, beyond the conventional state-of-the-art ALD processes, there is an increasing interest to develop different area-selective (AS) protocols in which the film growth can be selectively limited to certain predetermined surface areas only. Ideally, such AS-ALD approaches would allow the direct bottom-up fabrication of patterned active material components. One distinct advance that the BCPs can provide is the relatively large-area patterned templates of smaller domain sizes (down to appr. 5 nm) compared to those achievable with common photolithography techniques.[37]

A. Philip, Y. Dong, J. Vapaavuori, M. Karppinen
Department of Chemistry and Materials Science
Aalto University
FI-00076 Espoo, Finland
E-mail: jaana.vapaavuori@aalto.fi; maarit.karppinen@aalto.fi

The ORCID identification number(s) for the author(s) of this article can be found under https://doi.org/10.1002/adem.202300937.

DOI: 10.1002/adem.202300937

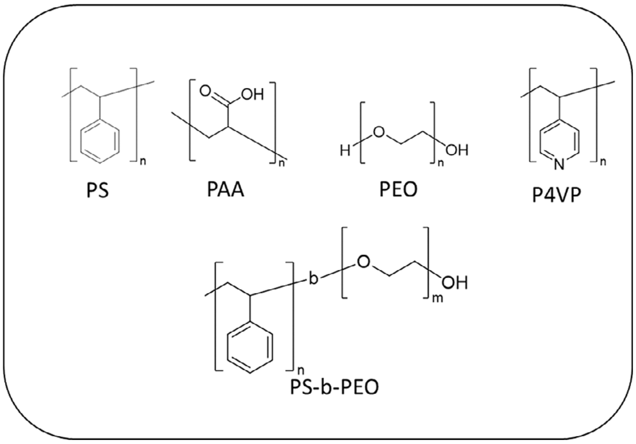

Figure 1. Chemical structures of PS, PAA, PEO, P4VP, and PS-*b*-PEO.

For ZnO films, the AS-ALD has been challenged utilizing, e.g., self-assembled monolayers (SAMs),[38,39] BCPs,[22,23] atomic-layer additive manufacturing,[40] biotemplates,[41,42] and even surface activation.[43]

In previous ALD studies, polyethylene terephthalate, polyethylene naphthalate, polystyrene, and Kapton have served as typical examples of flexible substrates.[7,44] In the present study, our aims were to 1) widen the polymer variety, 2) systematically investigate the ZnO growth on these different polymer surfaces and based on the gained understanding, and 3) design a BCP composed of two dissimilar polymers for the demonstration of area-selective growth of ZnO. The following four homopolymers were selected for this study: polystyrene (PS), polyacrylic acid (PAA), polyethylene oxide (PEO),[45] and poly(4-vinylpyridine) (P4VP), as these polymers are common constituents of BCPs; the chemical structures of these polymers are shown in **Figure 1**. Based on the initial screening results, we then selected PEO and PS as the constituents for the BCP substrates with two different block ratios.

2. Results and Discussion

2.1. Depositions on Homopolymer Substrates

We first investigated the ALD growth behavior of ZnO at 125 °C on the chosen four different homopolymer surfaces and for comparison also on a conventional silicon substrate surface. For every polymer, depositions with different cycle numbers between 100 and 500 were made. The observed GPC value of 2.2 Å cycle^{-1} in case of silicon substrate was similar to the previously reported values.[28] The observed growth rates on different polymers (**Figure 2**) indicate that the adsorption behavior of DEZ varies depending on the polymer. The lowest growth rate (0.85 Å cycle^{-1}) was observed for PEO. The GPC value obtained in case of PS (2.1 Å cycle^{-1}) was close to that of silicon and was the highest among the polymers investigated. Our contact angle measurements for the spin-coated homopolymer substrates showed that the PS surface was hydrophobic ($\theta_C \approx 90$) whereas the other substrates were hydrophilic ($\theta_C < 23$); this could be one of the explanations for the different growth rates. To fully understand the different surface reactivities, the importance of computational modeling efforts is emphasized here.

For PAA, in our initial tests the growth rate was found to be somewhat lower during the initial deposition cycles indicating

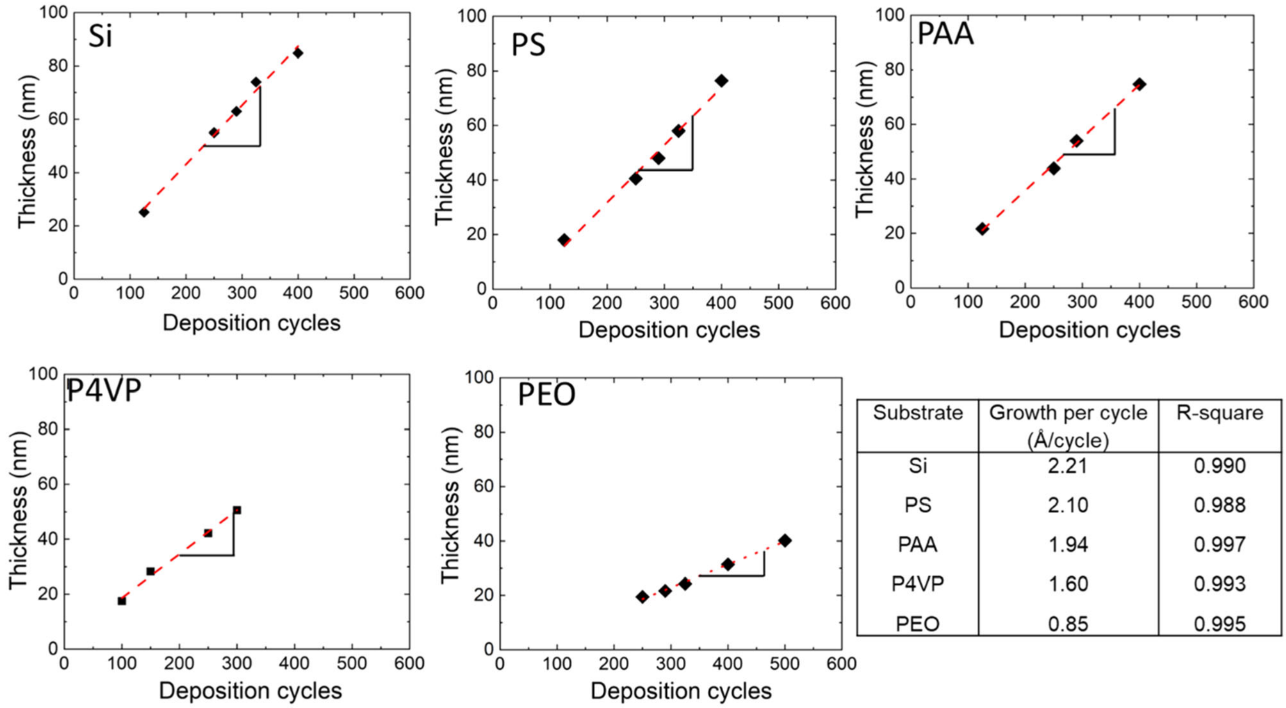

Substrate	Growth per cycle (Å/cycle)	R-square
Si	2.21	0.990
PS	2.10	0.988
PAA	1.94	0.997
P4VP	1.60	0.993
PEO	0.85	0.995

Figure 2. Linear dependence of film thickness on the number of ALD cycles applied on different substrate surfaces; the GPC values calculated from the slope of the fitted lines and corresponding R^2 values are given in the table.

there could be clear nucleation delay for the ZnO growth on this polymer substrate. In Figure 2, this is seen from the fact that the extrapolation of the thickness versus cycle number line to zero thickness crosses the cycle number axis at a value significantly deviation from zero. Similar nucleation delay with ZnO has been previously observed for some other polymers such as PMMA.[46] However, in our experiments no clear indications for the nucleation delay were seen for the other homopolymer substrates.

Another possible issue affecting the growth rate is the so-called vapor phase infiltration (VPI) phenomenon often seen for small precursor molecules such as trimethyl aluminum or DEZ especially when the substrate is a bulk polymer.[46,47] We investigated this by varying the deposition temperature for the PS polymer, and observed that the GPC increased with increasing deposition temperature (Figure S1, Supporting Information). This observed trend in the growth rate could be interpreted as a consequence of VPI. In some earlier studies,[22,23] it was found that the crystallinity difference between the constituent polymers in a BCP may play an important role in controlling the VPI, and thereby possibly also the area-selective growth of ZnO; the data were for a P3HT-*b*-PEO BCP, and the results revealed that the amorphous PEO was more prone for the diffusion of the precursors into the polymer (i.e., VPI) than the crystalline P3HT which more efficiently blocked the precursor diffusion. In our case, all other homopolymers were found amorphous while for the PEO polymer grazing-incidence X-ray diffraction (GIXRD) revealed some degree of crystallinity. Namely, for the PEO homopolymer a small diffraction peak at $2\theta = 17.95°$ ($d = 4.94$ Å) was evident, and accordingly we could assume that the diffusion of DEZ might be hindered into this PEO (in comparison to the amorphous polymers).

The GIXRD analyses (**Figure 3**) indicated that the ZnO film grows crystalline on all the substrates, but the underlying polymer clearly affects the film orientation. The (100) reflection of the ZnO wurtzite structure is dominant for the films grown on all other polymers except for PEO, for which the (002) reflection is dominant.[28]

Analysis of the samples using scanning electron microscopy (SEM) (**Figure 4**) clearly showed that ZnO grows as a continuous and homogeneous coating on all the investigated homopolymer substrates. The SEM analysis also indicated that the films consist of granular crystallites as previously reported for ALD-ZnO films,[48] even though the size and shape of the grains differ between the polymers. The grains were found to be bigger on PS as compared to the case of the Si or PEO substrates, in line with the observed sharper/more intense GIXRD peaks for the films grown on PS. In case of PAA, the ZnO grains were found to deviate from the usual granular shape toward a more spherical shape, and no grains were observed in case of P4VP. The low deposition temperature used here has obviously affected the grain size,[48] which may be the main reason for the relatively small grains observed in this study in general. Tentatively, we believe that the ZnO film morphology could relate to the film orientation.[48]

The knowledge obtained here for the influence of the underlining polymer substrate (along with the low deposition temperature) on the grain size and orientation of the ZnO films is important regarding their potential applications as these parameters should have an impact on the electrical transport properties.[49,50]

2.2. Depositions on BCPs

The fact that BCP thin films can be tailored to exhibit various self-assembly schemes in nanometer length scales resulting in unique surface patterns motivated us to challenge them in this study. Moreover, these surface patterns/characteristics can be easily controlled by varying fabrication parameters, such as withdrawal speed of dip coating and solvent of spin coating,[1,51] and also by the choice of the individual polymer components of BCPs, depending on the different application requirements. For the present study, our systematic experiments on the homopolymers gave us important design guidelines for the choice of the polymer components in our BCP substrates.

Based on the GPC values seen for the growth of ZnO on different polymers, we decided to fabricate the BCPs from PEO and PS, as they showed the lowest (0.85 Å cycle^{-1}) and highest (2.10 Å cycle^{-1}) growth rates, respectively. In this way, the substrates containing both easy-growth and limited-growth polymer components could be fabricated. Two BCPs with different ratios of PEO and PS were employed, i.e., PS-*b*-PEO with a higher proportional PS content, and PEO-*b*-PS with a higher proportional PEO content. With the help of cross-sectional SEM images

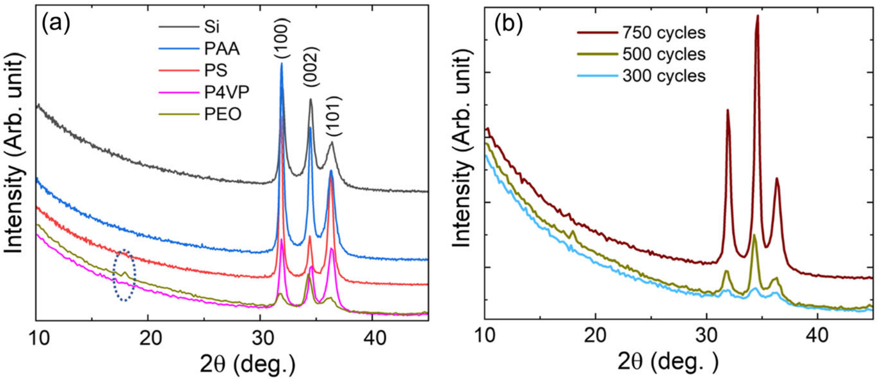

Figure 3. GIXRD patterns for ZnO films grown a) with 500 cycles on different substrates (different polymers and Si for comparison) and b) with different cycle numbers on PEO. The diffraction peak observed at $2\theta = 17.95^{\circ}$ for the sample grown on the PEO substrate originates from the substrate.

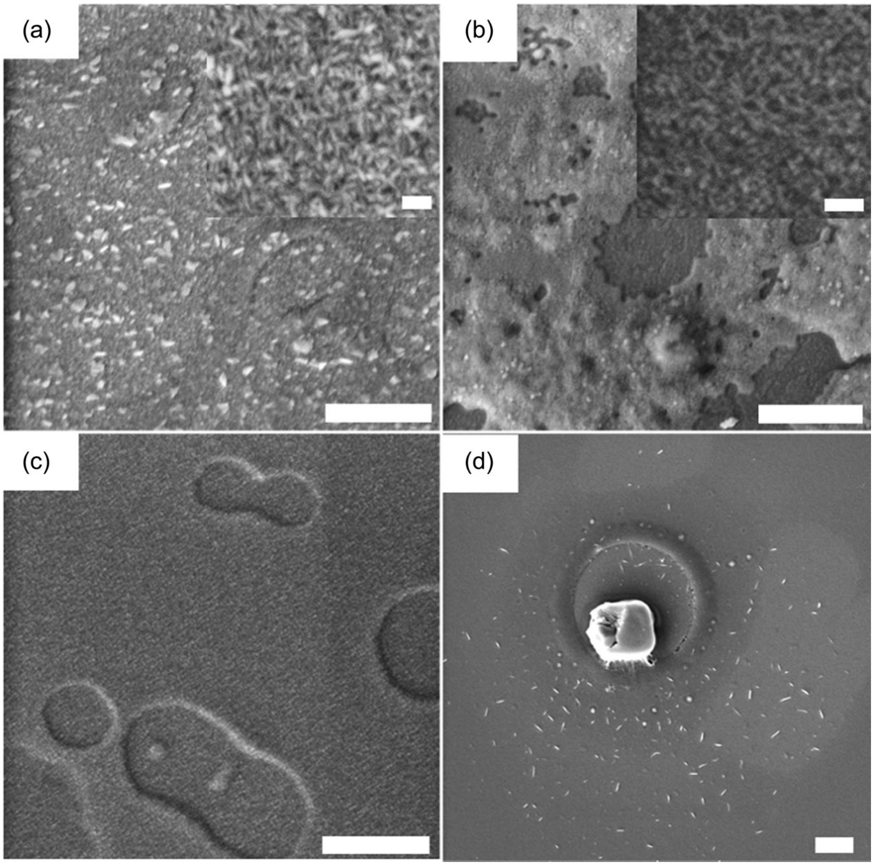

Figure 4. SEM images for ZnO films grown with 150 cycles on a) PS, b) PEO, c) PAA, and d) P4VP (scale bars: 1000 nm); insets in (a) and (b) are images for films grown with 500 cycles (scale bars: 100 nm).

(Figure S2, Supporting Information), we could estimate that both BCP films were around 100 nm thick.

The morphology of as-prepared PS-*b*-PEO film is shown in Figure S3, Supporting Information, which depicts a typical surface pattern resulting from the self-assembly of BCP without further treatment, whereas the PEO-*b*-PS presented a featureless surface. On the PS-*b*-PEO surface, the PEO parts form cylinder-type features embedded in the PS matrix. The ZnO depositions on these two different BCP substrates resulted in significantly different ZnO surface morphologies, as will be discussed in the following paragraphs.

The ALD parameters for the ZnO depositions on the BCP substrates were chosen to be essentially similar to those used for the individual polymer substrates. We opted for slightly higher cycle numbers (150–500) to get thicker films to better observe the differences in the growth rate on the different polymer parts. The resultant film thicknesses could not be determined with X-ray reflectivity (XRR) measurements, as the obtained patterns showed no fringes (different from the case of homopolymer substrates); this is naturally the outcome/indication of the patterned film surface, as aimed here for the BCPs. However, the gradual film thickness growth with the number of ALD cycles applied could be verified with the GIXRD measurements (**Figure 5**).

Even though ZnO apparently grows with different rates on PS and PEO, neither one of these surfaces is completely inert against it. Hence, it is not realistic to anticipate fully area-selective growth on the present BCP substrates. Nevertheless, looking at the 500-cycle GIXRD data (Figure 5), it is clear that the overall ZnO growth rate is significantly higher for PS-*b*-PEO for which the "easy-growth" PS areas dominate. Also, it is seen that compared to the film growth on PS, the presence of PEO inclusions in PS-*b*-PEO depresses the overall growth rate (GIXRD peak intensities); this is particularly clear for the initial deposition cycles (when the substrate effect is the largest).

Moreover, the film orientations on these two BCP substrates are in line with our expectations based on the results for the homopolymer substrates. While the ZnO coating grows on PS with a clear preference for the (100) orientation, for the ZnO coating on PS-*b*-PEO—besides the (100) reflection—also the (002) reflection is prominent. On the other hand, for the film grown on PEO-*b*-PS, the (002) reflection dominates (like in case of PEO). It is also clearly seen that, as the coating apparently grows thicker on the PS areas, the (100) reflection is also significantly strong. Especially with the higher cycle numbers the (100) reflection gets truly prominent, due to the higher growth rate of ZnO on PS in comparison to PEO.

The different growth rates on the PS and PEO areas in our BCP substrates were clearly observable from the atomic force microscopy (AFM) images as well. In **Figure 6**, AFM images are shown for both the uncoated and coated BCPs; the data

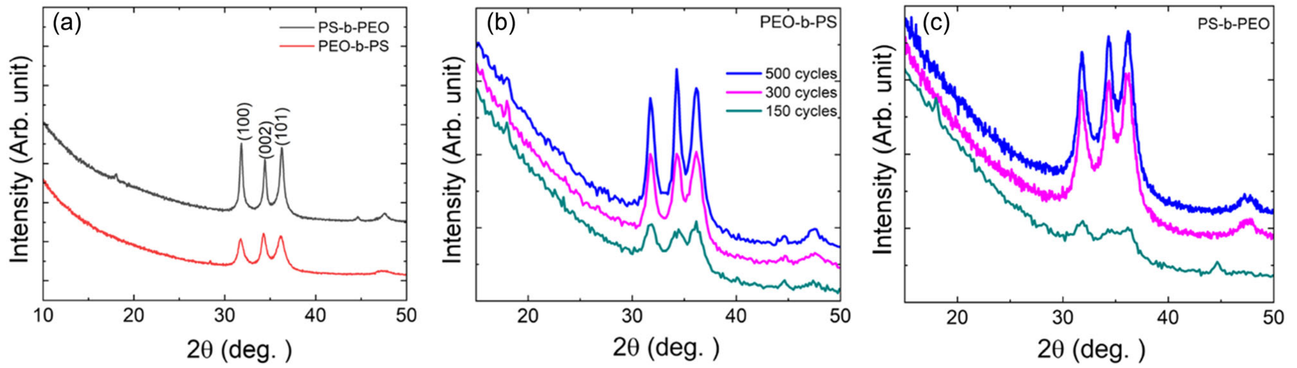

Figure 5. GIXRD of ZnO thin films grown on BCP: a) 500 cycles of ALD, b) different ALD cycles on PEO-*b*-PS, and c) different ALD cycles on PS-*b*-PEO.

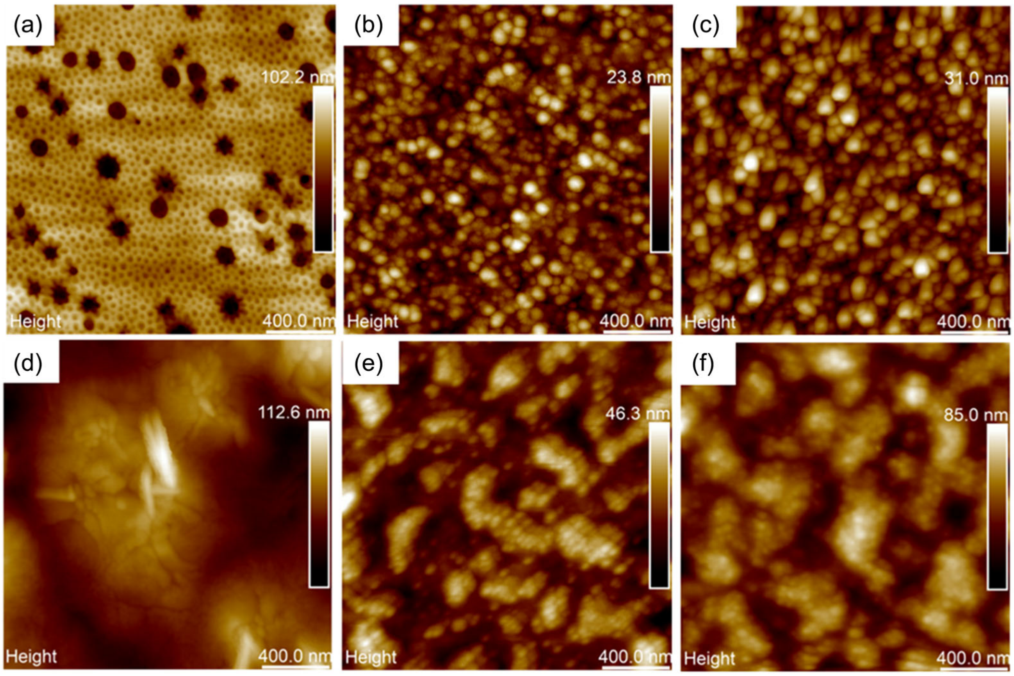

Figure 6. AFM images for a) plain PS-*b*-PEO substrate, and the same substrate coated with ZnO using b) 300 or c) 500 ALD cycles; d) Plain PEO-*b*-PS substrate, and the same substrate coated with ZnO using e) 300 or f) 500 ALD cycles. Scale bars embedded in images.

are, moreover, shown for two different ZnO coating thicknesses obtained with 300 and 500 ALD cycles. First of all, it is clear that the two plain BCPs exhibit different surface morphologies. For PS-*b*-PEO, the surface shows a uniform dot pattern (dots resulting from the organization of cylindrical domains of PEO; similar to the one reported for PS-*b*-PEO fabricated with a dip-coating technique[51]), while for PEO-*b*-PS a featureless surface without any specific pattern is seen.

The area-dependent growth is best seen for the PS-*b*-PEO substrate, as the surface looks dotted pattern (dots due to the "limited-growth" PEO areas) also after the ZnO deposition, reflecting the polymer-type dependent growth (Figure 6a–c). The higher content of limited-growth PEO in PEO-*b*-PS results in island-shaped patches upon the ZnO deposition with grains in agglomerated form.

In **Figure 7**, we display SEM images for both the uncoated and coated BCPs. The different surface morphologies of the two plain BCPs are evident from these SEM images as well. For PS-*b*-PEO, the uniform dot-patterned surface looks very similar to that seen for PLLA-*b*-PS,[52] while the PEO-*b*-PS surface is rather featureless. Images for the coated surfaces reveal that the grain shapes are quite different on the two different BCPs. In case of PS-*b*-PEO, the ZnO grains are granular (like on PS), whereas on PEO-*b*-PS the grains are spherical and clearly smaller in size. The film on PS-*b*-PEO appears essentially continuous, while on PEO-*b*-PS nearly noncoated areas are seen (due to the large portion of the limited-growth PEO areas) making the film discontinuous with small islands of closely packed grains.

We also characterized the different samples for their hydrophobicity. Owing to the higher content of hydrophobic

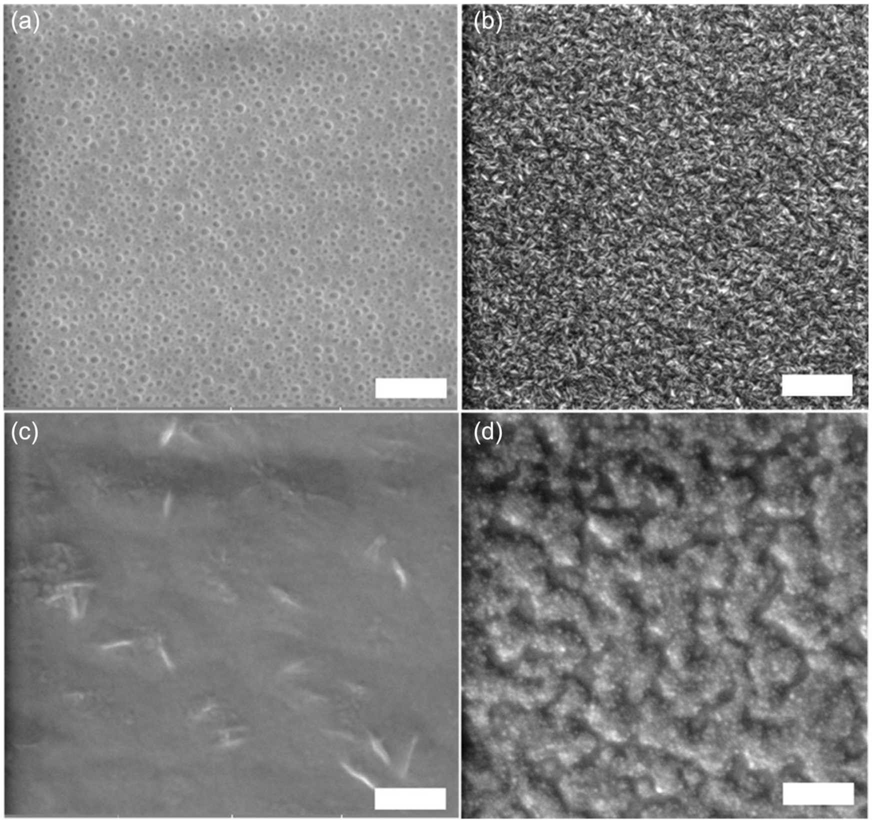

Figure 7. SEM images for a) plain PS-*b*-PEO substrate, b) PS-*b*-PEO coated with 500 ZnO ALD cycles, c) plain PEO-*b*-PS substrate, and d) PEO-*b*-PS coated with 500 ZnO ALD cycles. The scale bar in each image is 500 nm.

PS in the matrix, the PS-*b*-PEO substrate is highly hydrophobic with a contact angle of 80.5, whereas the contact angle of PEO-*b*-PS is only 59. Indeed, it seems that the major polymer constituent in the BCP controls its hydrophilic/hydrophobic nature. After the ZnO coating with 150 cycles, all the surfaces were found hydrophobic with the contact angle varying in the range of 72–96.[53] The ZnO coatings deposited on PEO-*b*-PS (or plain PEO) were found less hydrophobic than those on PS-*b*-PEO, indicating that the underlining hydrophilic PEO depresses the hydrophobicity of the ZnO layer grown on top of it.

Finally, we investigated the influence of the underlining polymer substrate on the electrical conductivity of the ZnO coating layer, which is important considering the potential applications of these films in flexible electronics. We conducted two-probe resistance measurements for the ZnO films deposited on different substrates with 500 ALD cycles (see **Table 1**). The results showed that on polymer surfaces the electrical conductivity of ZnO is always somewhat compromised in comparison to the similarly grown ZnO film on silicon. The resistivity values obtained indicate that among the polymers investigated, PS substrate tends to reduce the electrical conductivity of ZnO more strongly than the other polymers. This is seen not only for ZnO grown onto the plain PS substrate, but also for the BCPs, as the film grown on PEO-*b*-PS has lower resistance than the one grown on PS-*b*-PEO. This is interesting, taking into account that the ZnO growth rate on PS substrate was very close to the growth rate on Si. However, electrical conductivity of ZnO thin films depends—besides film thickness and crystallinity—also on the crystallite orientation such that the conductivity is expected to be highest for (002)-oriented films.[54,55]

Table 1. Resistance measured for ZnO films grown with 500 cycles on different polymer substrates.

Substrate	Resistance [MΩ]
Si	0.03
PAA	0.06
PEO	1.5
PMMA	4
P4VP	6
PS	11
PS_{5k}-*b*-PEO_{10k}	5
PS_{20k}-*b*-$PEO_{9.5k}$	20

3. Conclusions

We have systematically investigated the ALD growth of semiconducting ZnO films on various polymer surfaces. The underlining polymer substrate was shown to have a significant effect both on the growth rate and the properties of the ZnO coating, thus underlining the importance of the proper tailoring of the polymer surface when aiming at future flexible electronics applications.

Most importantly, a novel approach for selective ALD growth of ZnO coatings was introduced based on BCPs tailor-made from easy-growth and limited-growth polymer components, i.e., polystyrene and polyethylene oxide, respectively. In recent years, so-called inherent-type AS-ALD approaches have been developed,[56,57] with targets that are possibly closest to the goals of our BCP approach. Even though we could not demonstrate the perfect area-selectivity for the chosen BCPs, PS-*b*-PEO and PEO-*b*-PS, the results obtained provided us excellent proof-of-the-concept data for the validity of the approach. To realize the perfect selectivity, a polymer component with zero growth should be searched for. Nevertheless, even without the perfect selectivity, the BCP approach is capable in producing tailored nanoscale surface patterns; such nanopatterned/nanostructured materials are of significant application potential in, e.g., catalysis or thermoelectrics.

4. Experimental Section

The polymer surfaces investigated were fabricated on silicon wafers by spin coating using different polymer solutions. The chosen single-component polymers, PS ($M_w = 280\,000$, Sigma–Aldrich), PAA ($M_w = 1800$, Sigma–Aldrich), PEO ($M_v = 400\,000$, Sigma–Aldrich), and P4VP ($M_w = 3840$, Polymer Source) were dissolved in tetrahydrofuran (THF, ≥99.0% Sigma–Aldrich) as 0.1 wt% solutions at room temperature. Additionally, two PS-*b*-PEO BCPs were purchased (Polymer Source) with different dominated blocks, i.e., PS_{20k}-*b*-$PEO_{9.5k}$ (M_n (PS) = 20 kg mol^{-1} and M_n (PEO) = 9.5 kg mol^{-1}) and PS_{5k}-*b*-PEO_{10k} (M_n (PS) = 5 kg mol^{-1} and M_n (PEO) = 10 kg mol^{-1}); these BCPs are called PS-*b*-PEO and PEO-*b*-PS, respectively, to indicate first the majority component. In both cases, the 10 mg ml^{-1} solution was obtained by dissolving 0.05 g BCP into 5 mL THF at room temperature. To fabricate the polymer films on silicon, the solutions were spin-coated at 2000 rpm for 30 s (WS-650MZ-23NPPM 0 Laurell spin-coater). The polymer films were characterized for the thickness by XRR and contact angles (see **Table 2**). The P4VP, PEO, and PAA surfaces were found highly hydrophilic with a contact angle of less than 25 (P4VP being the most hydrophilic), while PS was hydrophobic with a contact angle higher than 90 in pristine condition.

All the ZnO film depositions were carried out in a Picosun R-100 ALD reactor, using DEZ (>52 wt% Zn basis from Sigma–Aldrich) and deionized water as precursors. Both precursors were placed outside the reactor in cylinders and pulsed at 21 °C. Nitrogen (99.999%; flow rate 300 SCCM) was used as both the carrier gas during the precursor pulses and the purge gas between the precursor pulses. The reactor pressure was kept at 3–5 mbar, and the depositions were carried out at 125 °C (substrate temperature). As substrates, $2.0 \times 2.0\ \text{cm}^2$ cuts of different polymers and also Si(100) (Okmetic Oy) for comparison were used. Following precursor pulse/purge lengths were used for the depositions: 0.3 s DEZ/9 s N_2/0.2 s H_2O/9 s N_2.

Table 2. Basic characteristics of the polymer substrates employed.

Polymer	Thickness [nm]	Contact angle
PS	7.6	90.7
PAA	9.7	23.2
PEO	11.2	22.6
P4VP	12.2	<10

All the films were characterized for their thickness with XRR (PANalytical X'Pert PRO Alfa 1) measurements; the data were fitted using the X'Pert reflectivity software by PANalytical. The same diffractometer was used to collect the GIXRD patterns for the films with an incident angle of 0.5°. Film morphologies were studied with SEM (Tescan Mira3) using an acceleration voltage of 5 kV. Before these investigations, the samples were sputtered with gold/palladium (80/20) on the surface. Moreover, in order to take a closer look at the grains, AFM (Bruker MultiMode 8) images were taken for selected samples. The AFM images were obtained with a J-scanner in a tapping mode. The static contact angle of a sessile drop of water on the samples was measured using an optical tensiometer (Biolin Scientific Theta Flex). For each measurement, a drop of 5 µL was dispensed on the surface and its image was captured using an in situ high-speed camera. The contact angle was determined by the software directly. Finally, for electrical resistivity measurements, a two-probe resistance method was used.

Supporting Information

Supporting Information is available from the Wiley Online Library or from the author.

Acknowledgements

A.P. and Y.D. contributed equally to this work. Funding was received through the Academy of Finland SUPER-WEAR project (decision number: 322214), and the European Research Council (H2020) StG "Autonomously adapting and communicating modular textiles" (grant no. 949648) and AdG "Unique ALD/MLD-enabled material functions" (grant no. 101097815). The authors also acknowledge the use of the RawMatTERS Finland Infrastructure (RAMI) at Aalto University.

Conflict of Interest

The authors declare no conflict of interest.

Data Availability Statement

The data that support the findings of this study are available from the corresponding author upon reasonable request.

Keywords

area-selective atomic-layer deposition, block copolymers, coatings, low-temperature ALD, zinc oxide

Received: June 19, 2023
Revised: September 21, 2023
Published online: September 29, 2023

[1] J. K. Kim, S. Y. Yang, Y. Lee, Y. Kim, *Prog. Polym. Sci.* **2010**, *35*, 1325.
[2] C. Li, Q. Li, Y. V. Kaneti, D. Hou, Y. Yamauchi, Y. Mai, *Chem. Soc. Rev.* **2020**, *49*, 4681.
[3] C. Cummins, R. Lundy, J. J. Walsh, V. Ponsinet, G. Fleury, M. A. Morris, *Nano Today* **2020**, *35*, 100936.
[4] I. Botiz, S. B. Darling, *Mater. Today* **2010**, *13*, 42.
[5] J. Bang, U. Jeong, D. Y. Ryu, T. P. Russell, C. J. Hawker, *Adv. Mater.* **2009**, *21*, 4769.
[6] H. G. Yoo, M. Byun, C. K. Jeong, K. J. Lee, *Adv. Mater.* **2015**, *27*, 3982.

[7] V. Zardetto, T. M. Brown, A. Reale, A. di Carlo, *J. Polym. Sci., Part B: Polym. Phys.* **2011**, *49*, 638.
[8] T. Tynell, M. Karppinen, *Semicond. Sci. Technol.* **2014**, *29*, 043001.
[9] H. Kim, M. J. Jung, S. Choi, B. J. Choi, *J. Electron. Mater.* **2021**, *50*, 1955.
[10] C. Otalora, M. A. Botero, G. Ordoñez, *J. Mater. Sci.* **2021**, *56*, 15538.
[11] B. Macco, W. M. M. Kessels, *Appl. Phys. Rev.* **2022**, *9*, 041313.
[12] A. Omerzu, R. Peter, D. Jardas, I. Turel, K. Salamon, M. Podlogar, D. Vengust, I. Jelovica Badovinac, I. Kavre Piltaver, M. Petravic, *Surf. Interfaces* **2021**, *23*, 100984.
[13] V. K. Arepalli, W. J. Lee, Y. D. Chung, J. Kim, *Mater. Sci. Semicond. Process.* **2021**, *121*, 105406.
[14] C. Battaglia, J. Escarré, K. Söderström, M. Charrière, M. Despeisse, F. J. Haug, C. Ballif, *Nat. Photonics* **2011**, *5*, 535.
[15] S. O'Brien, M. G. Nolan, M. Çopuroglu, J. A. Hamilton, I. Povey, L. Pereira, R. Martins, E. Fortunato, M. Pemble, *Thin Solid Films* **2010**, *518*, 4515.
[16] T. Suntola, *Mater. Sci. Rep.* **1989**, *4*, 261.
[17] R. W. Johnson, A. Hultqvist, S. F. Bent, *Mater. Today* **2014**, *17*, 236.
[18] J. R. Bakke, K. L. Pickrahn, T. P. Brennan, S. F. Bent, *Nanoscale* **2011**, *3*, 3482.
[19] S. M. George, *Chem. Rev.* **2010**, *110*, 111.
[20] J. Ahn, C. Ahn, S. Jeon, J. Park, *Appl. Sci.* **2019**, *9*, 1990.
[21] L. Yao, L. E. Oquendo, M. W. Schulze, R. M. Lewis, W. L. Gladfelter, M. A. Hillmyer, *ACS Appl. Mater. Interfaces* **2016**, *8*, 7431.
[22] M. Moshonov, Y. Kauffmann, G. L. Frey, *Polymer* **2016**, *105*, 214.
[23] M. Moshonov, G. L. Frey, *Langmuir* **2015**, *31*, 12762.
[24] H. S. Moon, J. Y. Kim, H. M. Jin, W. J. Lee, H. J. Choi, J. H. Mun, Y. J. Choi, S. K. Cha, S. H. Kwon, S. O. Kim, *Adv. Funct. Mater.* **2014**, *24*, 4343.
[25] M. A. Hareri, D. J. H. Emslie, *Chem. Mater.* **2022**, *34*, 2400.
[26] K. Yoshida, I. Nagata, K. Saito, M. Miura, K. Kanomata, B. Ahmmad, S. Kubota, F. Hirose, *J. Vac. Sci. Technol., A* **2022**, *40*, 022408.
[27] M. Kot, L. Kegelmann, C. Das, P. Kus, N. Tsud, I. Matolinova, S. Albrecht, V. Matolin, D. Schmeisser, *ChemSusChem* **2018**, *11*, 3640.
[28] J. Malm, E. Sahramo, J. Perälä, T. Sajavaara, M. Karppinen, *Thin Solid Films* **2011**, *519*, 5319.
[29] T. Hirvikorpi, M. Vähä-Nissi, T. Mustonen, E. Iiskola, M. Karppinen, *Thin Solid Films* **2010**, *518*, 2654.
[30] N. Poonkottil, H. Rijckaert, K. Rajendran, R. R. Petit, L. I. D. J. Martin, D. Van Thourhout, I. Van Driessche, C. Detavernier, J. Dendooven, *Adv. Mater. Interfaces* **2023**, *10*, 2201934.
[31] G. N. Parsons, S. E. Atanasov, E. C. Dandley, C. K. Devine, B. Gong, J. S. Jur, K. Lee, C. J. Oldham, Q. Peng, J. C. Spagnola, P. S. Williams, *Coord. Chem. Rev.* **2013**, *257*, 3323.
[32] L. Keskiväli, P. Heikkilä, E. Kenttä, T. Virtanen, H. Rautkoski, A. Pasanen, M. Vähä-nissi, M. Putkonen, *Coatings* **2021**, *11*, 1028.
[33] L. Mai, F. Mitschker, C. Bock, A. Niesen, E. Ciftyurek, D. Rogalla, J. Mickler, M. Erig, Z. Li, P. Awakowicz, K. Schierbaum, A. Devi, *Small* **2020**, *16*, 1907506.
[34] T. Hirvikorpi, M. Vähä-Nissi, A. Harlin, M. Karppinen, *Thin Solid Films* **2010**, *518*, 5463.
[35] T. Hirvikorpi, M. Vähä-Nissi, A. Harlin, J. Marles, V. Miikkulainen, M. Karppinen, *Appl. Surf. Sci.* **2010**, *257*, 736.
[36] T. Hirvikorpi, M. Vähä-Nissi, A. Harlin, M. Salomäki, S. Areva, J. T. Korhonen, M. Karppinen, *Appl. Surf. Sci.* **2011**, *257*, 9451.
[37] T. H. Epps, R. K. O'Reilly, *Chem. Sci.* **2016**, *7*, 1674.
[38] F. S. M. Hashemi, S. F. Bent, *Adv. Mater. Interfaces* **2016**, *3*, 1600464.
[39] J. Yarbrough, A. B. Shearer, S. F. Bent, *J. Vac. Sci. Technol., A* **2021**, *39*, 021002.
[40] S. Stefanovic, N. Gheshlaghi, D. Zanders, I. Kundrata, B. Zhao, M. K. S. Barr, M. Halik, A. Devi, J. Bachmann, *Small* **2023**, *19*, 2301774.
[41] J. Malm, E. Sahramo, M. Karppinen, R. H. A. Ras, *Chem. Mater.* **2010**, *22*, 3349.
[42] R. H. A. Ras, E. Sahramo, J. Malm, J. Raula, M. Karppinen, *J. Am. Chem. Soc.* **2008**, *130*, 11252.
[43] K. K. Mentel, A. V. Emelianov, A. Philip, A. Johansson, M. Karppinen, M. Pettersson, *Adv. Mater. Interfaces* **2022**, *9*, 2201110.
[44] A. Mathur, D. Pal, S. Chattopadhyay, *Macromol. Symp.* **2017**, *376*, 1600210.
[45] M.Á. Lorente, G. González-Gaitano, J. González-Benito, *Polymers* **2022**, *14*, 1299.
[46] M. Napari, J. Malm, R. Lehto, J. Julin, K. Arstila, T. Sajavaara, M. Lahtinen, *J. Vac. Sci. Technol., A* **2015**, *33*, 01A128.
[47] I. Azpitarte, G. A. Botta, C. Tollan, M. Knez, *RSC Adv.* **2020**, *10*, 15976.
[48] S. H. K. Park, Y. E. Lee, *J. Mater. Sci.* **2004**, *39*, 2195.
[49] J. H. Lee, Y. H. Kim, S. J. Ahn, T. H. Ha, H. S. Kim, *Mater. Sci. Eng., B* **2015**, *199*, 37.
[50] C. W. Nan, A. Tschöpe, S. Holten, H. Kliem, R. Birringer, *J. Appl. Phys.* **1999**, *85*, 7735.
[51] H. M. Nguyen, A. V. Mader, S. De, J. Vapaavuori, *Nanoscale Adv.* **2021**, *3*, 4996.
[52] E. Ji, C. Cummins, G. Fleury, *Molecules* **2021**, *26*, 1412.
[53] P. Y. Dave, K. H. Patel, K. V. Chauhan, A. K. Chawla, S. K. Rawal, *Procedia Technol.* **2016**, *23*, 328.
[54] M. Ohyama, H. Kozuka, T. Yoko, *J. Am. Ceram. Soc.* **1998**, *81*, 1622.
[55] N. P. Dasgupta, S. Neubert, W. Lee, O. Trejo, J. R. Lee, F. B. Prinz, *Chem. Mater.* **2010**, *22*, 4769.
[56] C. Zhang, M. Vehkamäki, M. Leskelä, M. Ritala, *Dalton Trans.* **2023**, *52*, 9622.
[57] J. Lee, J. M. Lee, H. Oh, C. Kim, J. Kim, D. H. Kim, B. Shong, T. J. Park, W. H. Kim, *Adv. Funct. Mater.* **2021**, *31*, 2102556.